International Journal of Bifurcation and Chaos, Vol. 3, No. 6 (1993) 1629–1638

ROBUSTNESS AND SIGNAL RECOVERY IN A SYNCHRONIZED CHAOTIC SYSTEM

KEVIN M. CUOMO and ALAN V. OPPENHEIM
Research Laboratory of Electronics and the Department of Electrical Engineering and Computer Science, MIT, Cambridge, MA 02139, USA
STEVEN H. STROGATZ
Department of Mathematics, MIT, Cambridge, MA 02139, USA

Received October 7, 1993

Recent papers have demonstrated that synchronization in the Lorenz system is highly robust to additive perturbation of the drive signal. This property has led to a concept known as chaotic signal masking and recovery. This paper presents experiments and an approximate analytical model that quantify and explain the observed robustness of synchronization in the Lorenz system. In particular, we explain why speech and other narrowband perturbations can be recovered faithfully, even though the synchronization error is comparable in power to the message itself.

1. Introduction

Chaotic signals are typically broadband, noise-like, and difficult to predict. These properties have led to the proposal that chaotic signals might be potentially useful in certain private communications contexts, e.g. as masks for information-bearing waveforms, and as modulating waveforms in spread spectrum systems [Oppenheim *et al.*, 1992]. These proposed approaches exploit the self-synchronization property of certain chaotic systems [Pecora & Carroll, 1990, 1991; Carroll & Pecora, 1991]. Synchronization, however, is not sufficient; the proposed applications also inherently require the robustness of the synchronization to perturbations of the synchronizing drive signal. Specifically, additive signal masking and recovery as described in Oppenheim *et al.*, [1992] relies on adding a low-level message signal to the synchronizing drive signal, and using this perturbed drive signal at the receiver to regenerate a clean drive signal. Through subtraction, the message is then recovered. The successful use of the Lorenz system for masking of speech signals has been previously demonstrated and reported, both as a simulation and as an analog circuit realization [Cuomo & Oppenheim, 1993; Cuomo *et al.*, 1993]. An analog circuit implementation of masking of a narrowband signal has also separately been demonstrated [Kocarev *et al.*, 1992].

This paper was motivated by a desire to understand the mechanism underlying the robustness. When a message or other perturbation is added to the chaotic drive signal, the receiver does not regenerate a perfect replica of the drive; there is always some synchronization error. Successful message recovery would result if the synchronization error was small relative to the perturbation itself. One of our main results is that for the Lorenz system, the synchronization error is *not* small compared to the perturbation; nevertheless, the message can be recovered because the synchronization error turns out to be nearly *coherent* with the message. We will present experimental evidence for this effect, along

with an explanation in terms of an approximate analytical model.

In Sec. 2, we summarize the use of the Lorenz system for signal masking and recovery. In Sec. 3, we describe the results of several experiments which demonstrate and evaluate the sensitivity of the synchronization. In Sec. 4, we present an approximate analytical error model which is consistent with and predicts the experimental results in Sec. 3. In Sec. 5, we compare the performance of the model to the experimental results.

2. Background

The Lorenz equations are given by

$$\begin{aligned} \dot{x} &= \sigma(y - x)\,, \\ \dot{y} &= rx - y - xz\,, \\ \dot{z} &= xy - bz\,, \end{aligned} \tag{1}$$

where σ, r, and b are parameters. The equations representing the synchronizing receiver are given by

$$\begin{aligned} \dot{x}_r &= \sigma(y_r - x_r)\,, \\ \dot{y}_r &= rs(t) - y_r - s(t)z_r\,, \\ \dot{z}_r &= s(t)y_r - bz_r\,, \end{aligned} \tag{2}$$

where $s(t)$ is the received drive signal. With $s(t)$ equal to the transmitter signal $x(t)$, the signals x_r, y_r, and z_r will asymptotically synchronize to x, y, and z, respectively [Cuomo & Oppenheim, 1993].

In signal processing applications it is typically of interest to adjust the time scale of the signals. This is accomplished in a straightforward way by establishing the convention that $\dot{x}$, $\dot{y}$, and $\dot{z}$ denote $dx/d\tau$, $dy/d\tau$, and $dz/d\tau$ respectively where $\tau = t/T$ is normalized time and T is a time scale factor. It is also convenient to define the normalized frequency $\omega = \Omega T$, where Ω denotes the angular frequency in units of rad/s. In the implementation reported in Cuomo & Oppenheim [1993] and the circuit experiments presented in this paper, the parameter values used where $T = 400$ μsec, $\sigma = 16$, $r = 45.6$, and $b = 4$.

Practical applications of the principle of synchronization require a certain robustness, i.e. the ability of the receiver to synchronize even when $s(t)$ differs slightly from $x(t)$, either unintentionally due to transmission effects or intentionally as in signal masking. Specifically, the use of this system for signal masking relies on the ability of the receiver signal $x_r(t)$ to approximately synchronize to the transmitter signal $x(t)$ when a perturbation $p(t)$ is added to $x(t)$, i.e. when $s(t)$ is given by

$$s(t) = x(t) + p(t)\,,$$

where $p(t)$ is the desired message to be transmitted and recovered. In this context, the recovered message is

$$\hat{p}(t) = s(t) - x_r(t) = p(t) + [x(t) - x_r(t)]\,.$$

In the following sections we examine the error between the state variables x, y, and z in the transmitter and the state variables x_r, y_r, and z_r in the receiver. The corresponding errors will be denoted as e_x, e_y, and e_z respectively, i.e.

$$\begin{aligned} e_x(t) &= x(t) - x_r(t)\,, \\ e_y(t) &= y(t) - y_r(t)\,, \\ e_z(t) &= z(t) - z_r(t)\,. \end{aligned} \tag{3}$$

In the specific application of signal masking, $e_x(t)$ corresponds directly to the error in the recovered message. In the next section, we present experimental results on the synchronization error when $p(t)$ is white noise and when $p(t)$ is a speech signal.

3. Experimental Demonstrations of Robustness

3.1. *Sensitivity of synchronization to additive white noise*

In this set of experiments, the perturbation $p(t)$ is Gaussian white noise. We denote by σ_x^2, σ_y^2, σ_z^2, and σ_p^2 the average power in $x(t)$, $y(t)$, $z(t)$, and $p(t)$ respectively. The input chaos-to-perturbation ratio (CPR) reflects the perturbation in the drive signal and is given by

$$\text{Input CPR} = 10 \log_{10}\left[\frac{\sigma_x^2}{\sigma_p^2}\right]. \tag{4}$$

The output chaos-to-error ratio (CER) associated with $x(t)$ reflects the error between $x(t)$ and $x_r(t)$ and is defined as

$$\text{Output CER}_x = 10 \log_{10}\left[\frac{\sigma_x^2}{\sigma_{ex}^2}\right]. \tag{5}$$

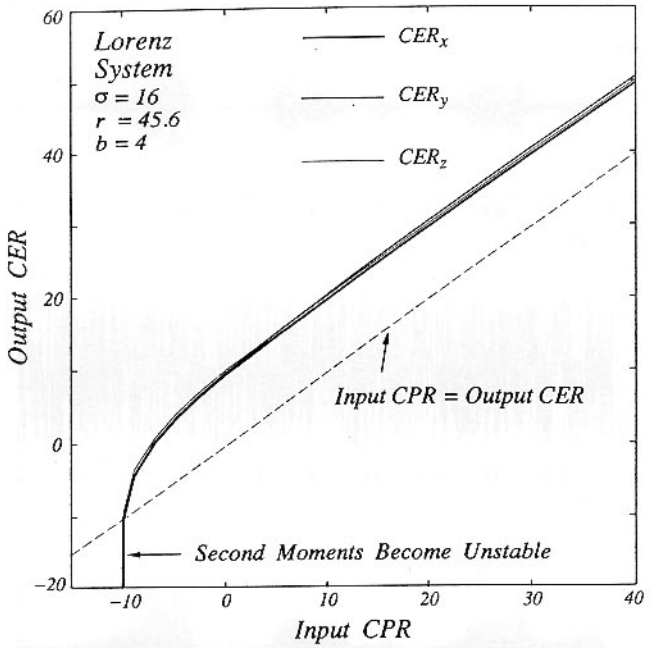

Fig. 1. Output CER_x, CER_y, and CER_z vs. Input CPR for the Lorenz synchronizing receiver.

The output CER for the state variables $y(t)$ and $z(t)$ are similarly defined as

$$\text{Output CER}_y = 10 \log_{10} \left[\frac{\sigma_y^2}{\sigma_{ey}^2} \right],$$

$$\text{Output CER}_z = 10 \log_{10} \left[\frac{\sigma_z^2}{\sigma_{ez}^2} \right].$$

Figure 1 shows a plot of output CER for each state variable as the input CPR is varied over a wide range. These data were generated by numerically integrating the transmitter and receiver equations and computing the error signals from Eqs. (3). Note that a threshold effect is evident at low input CPRs. However, above the threshold the behavior of the receiver appears to be robust. In particular above the threshold, and with $p(t)$ as wideband noise, the normalized error in synchronization of each of the state variables is approximately 10 dB less than the normalized error in the drive signal $x(t)$.

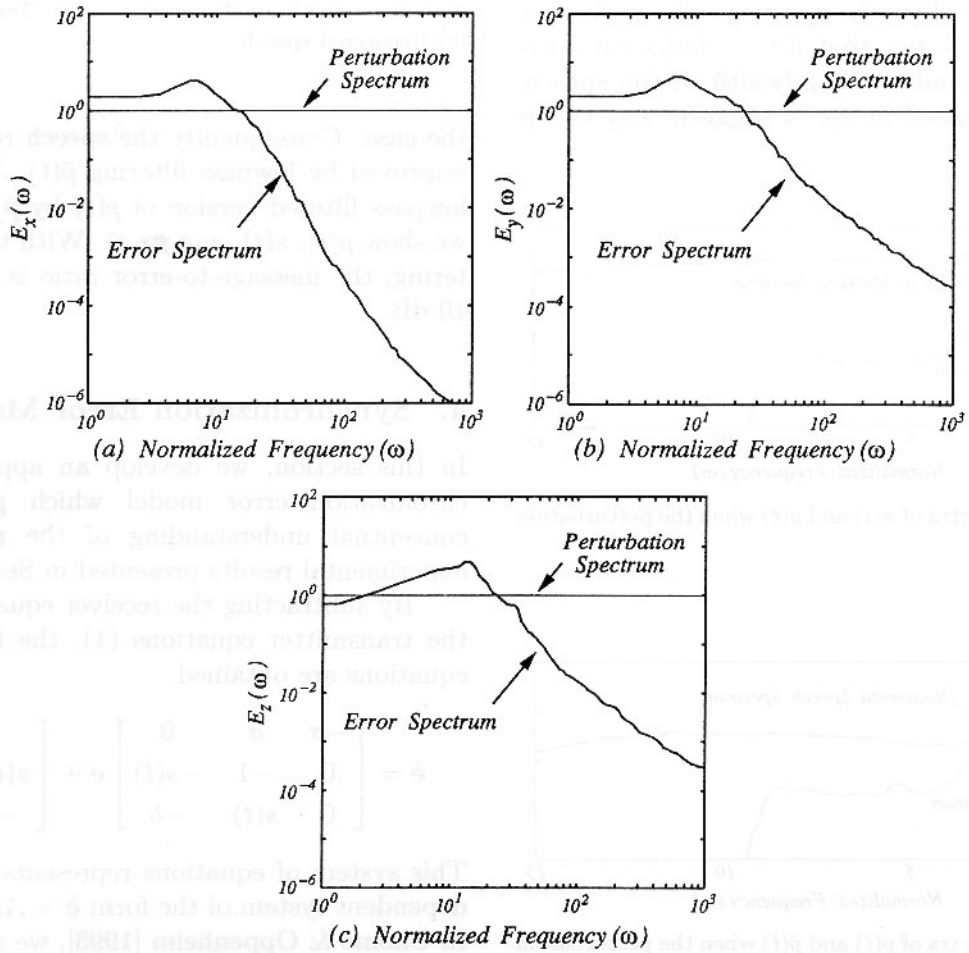

Fig. 2. True power spectra of the error signals: (a) $E_x(\omega)$. (b) $E_y(\omega)$. (c) $E_z(\omega)$.

In Fig. 2, we plot the message and error spectra for each of the three state variables vs. normalized frequency ω. We note that at relatively low frequencies, the error in reconstructing $x(t)$ slightly exceeds the perturbation of the drive but that for normalized frequencies above 20 the situation quickly reverses. The analytical model developed in Sec. 4 closely predicts this behavior.

3.2. *Sensitivity of synchronization to additive speech*

In this set of experiments, the analog circuit implementation of the Lorenz equations described in Cuomo & Oppenheim [1993] is used to demonstrate the robustness of the synchronization when $p(t)$ is a speech signal. The normalizing time parameter T is 400 μsec and the speech signal $p(t)$ is bandlimited to 4 kHz or equivalently to a normalized frequency ω of 10. Figure 3 shows the power spectrum of a representative speech signal $p(t)$ and the chaotic masking signal $x(t)$. The overall CPR in this experiment is approximately 20 dB.

In Fig. 4 we show the spectrum of $\hat{p}(t)$ for this same example. Notice that $\hat{p}(t)$ includes considerable energy beyond the bandwidth of the speech. The model discussed in Sec. 4 suggests why this is

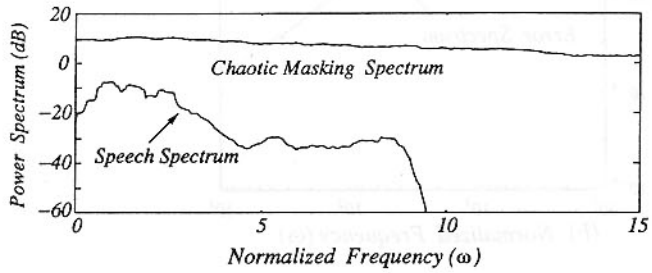

Fig. 3. Power spectra of $x(t)$ and $p(t)$ when the perturbation is a speech signal.

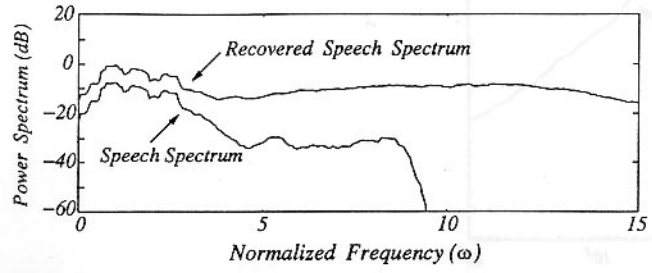

Fig. 4. Power spectra of $p(t)$ and $\hat{p}(t)$ when the perturbation is a speech signal.

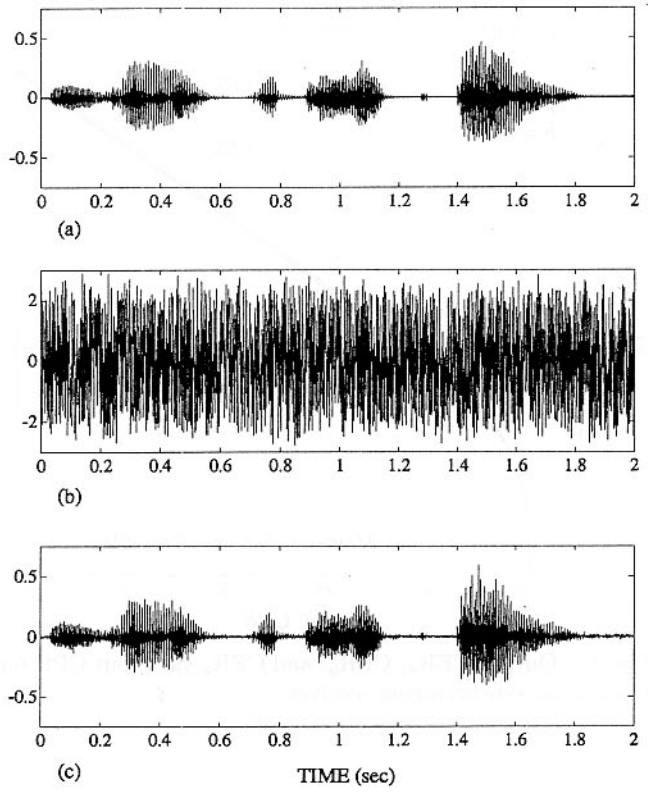

Fig. 5. (a) Original speech. (b) Transmitted signal. (c) Recovered speech.

the case. Consequently the speech recovery can be improved by lowpass filtering $\hat{p}(t)$. We denote the lowpass filtered version of $\hat{p}(t)$ by $\hat{p}_f(t)$. In Fig. 5 we show $p(t)$, $s(t)$, and $\hat{p}_f(t)$. With this lowpass filtering, the message-to-error ratio is approximately 10 dB.

4. Synchronization Error Model

In this section, we develop an approximate synchronization error model which provides some conceptual understanding of the numerical and experimental results presented in Sec. 3.

By subtracting the receiver equations (2) from the transmitter equations (1), the following error equations are obtained.

$$\dot{\mathbf{e}} = \begin{bmatrix} -\sigma & \sigma & 0 \\ 0 & -1 & -s(t) \\ 0 & s(t) & -b \end{bmatrix} \mathbf{e} + \begin{bmatrix} 0 \\ z(t) - r \\ -y(t) \end{bmatrix} p(t)$$

This system of equations represents a linear time-dependent system of the form $\dot{\mathbf{e}} = A(t)\mathbf{e} + \mathbf{b}(t)p(t)$. In Cuomo & Oppenheim [1993], we showed analytically that the error system is asymptotically stable

at the origin provided that σ, $b > 0$ and $p(t) = 0$. Clearly, this is not true for $p(t) \neq 0$, because the error system is driven by the perturbation $p(t)$ in this case.

It is useful in our subsequent analysis to rewrite the error equations in the form

$$\dot{\mathbf{e}} = \begin{bmatrix} -\sigma & \sigma & 0 \\ 0 & -1 & 0 \\ 0 & 0 & -b \end{bmatrix} \mathbf{e} + \begin{bmatrix} 0 \\ -e_z \\ e_y \end{bmatrix} s(t) + \begin{bmatrix} 0 \\ \nu(t) + \bar{z} - r \\ -y(t) \end{bmatrix} p(t), \tag{6}$$

where

$$\nu(t) = z(t) - \bar{z}.$$

The constant $\bar{z}$ denotes the mean value of $z(t)$. For the parameter values that we have chosen, the value of $\bar{z} \approx 39$.

Our approach to analyzing the error system (6) is to assume that:

- the perturbation $p(t)$ is small, i.e. $\sigma_p^2 \ll \sigma_x^2$;
- $\nu(t)$ is white noise; and
- $x(t)$ and $y(t)$ can be approximated by binary-valued functions with random transition times.

The first assumption is straightforward and allows us to approximate $s(t)$ by $x(t)$ in Eq. (6). The second assumption is justified by numerical experiment. While the third assumption may seem to be a very crude approximation, it is nevertheless a helpful heuristic. To make it more plausible, consider a sample function of $x(t)$ and $y(t)$ as illustrated in Figs. 6(a) and 6(b) respectively. A notable characteristic of these signals is that $x(t)$ resembles a scaled and slightly delayed version of $y(t)$. This similarity is consistent with the Lorenz equations (1) which indicate that $x(t)$ is the result of processing $y(t)$ with a lowpass filter having a cutoff frequency ω equal to σ. The binary-valued functions (dashed lines) in Figs. 6(a) and 6(b) emphasize the bipolar nature of these signals. The amplitude of these functions is scaled to reflect the standard deviation while the transition times occur at the zero crossings of the underlying waveform. The zero crossings of $x(t)$ and $y(t)$ appear to be randomly distributed and nearly coincide with each other. This suggests that we can approximate $x(t)$ and $y(t)$ by

$$x(t) \approx \sigma_x w(t),$$
$$y(t) \approx \sigma_y w(t),$$

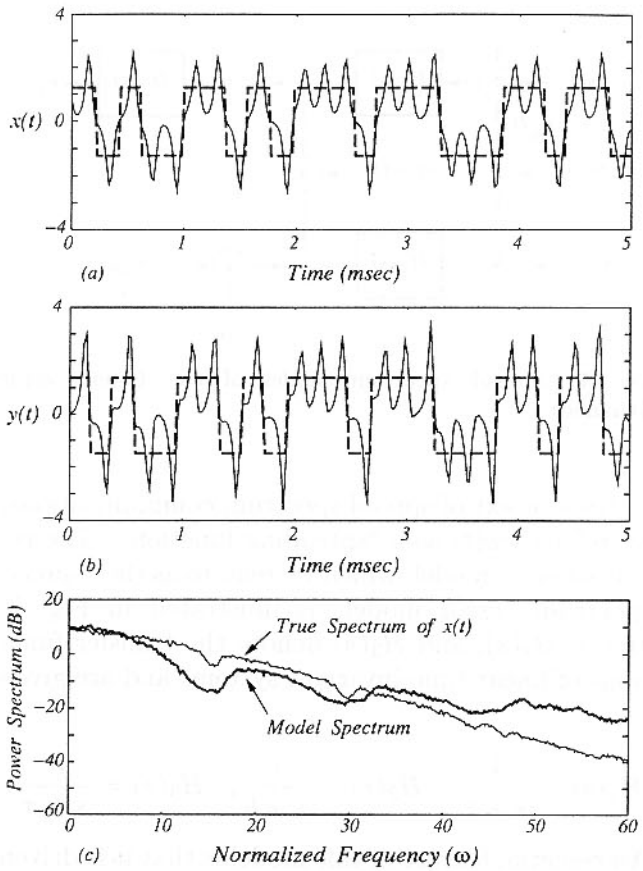

Fig. 6. (a) A sample function of $x(t)$. (b) A sample function of $y(t)$. (c) Power spectra of $x(t)$ and the piecewise constant approximation of $x(t)$.

where $w(t) = \pm 1$ with randomly distributed transition times. The power spectrum of $w(t)$ is broadband because of the random transition times and, as depicted in Fig. 6(c), reasonably approximates the power spectrum of the underlying waveforms. Because $w(t)$ is broadband, modulation of a narrowband signal with $w(t)$ will significantly increase the bandwidth of the narrowband signal. On the other hand, since $w^2(t) = 1$, the original narrowband signal can be exactly recovered by modulating with $w(t)$ a second time.

With these assumptions, Eq. (6) becomes

$$\dot{\mathbf{e}} = \begin{bmatrix} -\sigma & \sigma & 0 \\ 0 & -1 & 0 \\ 0 & 0 & -b \end{bmatrix} \mathbf{e} + \begin{bmatrix} 0 \\ -e_z \\ e_y \end{bmatrix} \sigma_x w(t) + \begin{bmatrix} 0 \\ \nu(t) + \bar{z} - r \\ -\sigma_y w(t) \end{bmatrix} p(t). \tag{7}$$

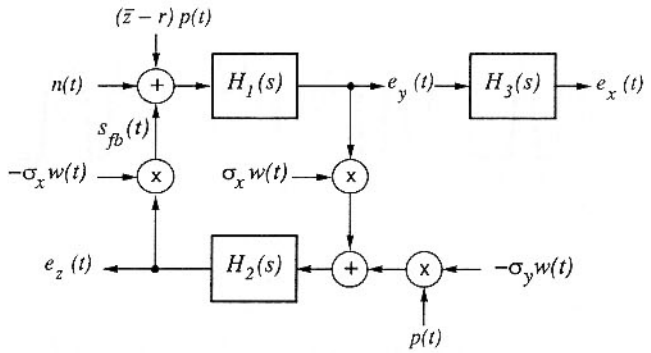

Fig. 7. Spread spectrum model of the Lorenz error dynamics.

In the context of spread spectrum communications, we refer to $w(t)$ as a "spreading function." The resulting error model, which we refer to as the "spread spectrum" error model, is illustrated in Fig. 7. $H_1(s)$, $H_2(s)$, and $H_3(s)$ denote the transfer functions of linear time-invariant systems and are given by

$$H_1(s) = \frac{1}{s+1}, \quad H_2(s) = \frac{1}{s+b}, \quad H_3(s) = \frac{\sigma}{s+\sigma}.$$

An essential feature of this model is that it is driven by the scaled perturbation $(\bar{z}-r)p(t)$ and a white noise signal $n(t) = \nu(t)p(t)$ having an intensity that depends on $p(t)$. We are now going to make a plausibility argument that $s_{fb}(t)$ contains the message $p(t)$. First, observe that the modulated signals $-\sigma_y w(t)p(t)$ and $\sigma_x w(t)e_y(t)$ are also broadband because $p(t)$ and $e_y(t)$ are modulated by the broadband spreading function $w(t)$. If these modulated signals were directly modulated by $w(t)$ a second time, then it would be possible to exactly recover $p(t)$ and $e_y(t)$ respectively. In Fig. 7, we see that $e_z(t)$ is the result of lowpass filtering the sum $-\sigma_y w(t)p(t)+\sigma_x w(t)e_y(t)$ with $H_2(s)$. It seems reasonable that the feedback signal $s_{fb}(t) = -\sigma_x w(t)e_z(t)$ will approximate a weighted sum of $p(t)$ and $e_y(t)$. This heuristic argument is consistent with numerical experiments and allows the error signals $e_y(t)$ and $e_x(t)$ to be viewed as consisting of the sum of a noise component due to lowpass filtering $n(t)$ and a component due to lowpass filtering the perturbation $p(t)$. As we show below, this interpretation of the error signals can be made more rigorous by adding an additional constraint.

In our subsequent analysis, it is useful to view Eq. (7) as two subsystems:

$$\dot{e}_x = \sigma(e_y - e_x), \tag{8}$$

and

$$\begin{bmatrix} \dot{e}_y \\ \dot{e}_z \end{bmatrix} = \begin{bmatrix} -1 & -\sigma_x w(t) \\ \sigma_x w(t) & -b \end{bmatrix} \begin{bmatrix} e_y \\ e_z \end{bmatrix} + \begin{bmatrix} n(t) + (\bar{z}-r)p(t) \\ -\sigma_y w(t)p(t) \end{bmatrix}. \tag{9}$$

The first subsystem (8) is a linear time-invariant system. The second subsystem (9) is also linear but has a time-dependent coefficient $w(t)$. Exploiting the linearity of these subsystems, we can write the solution to (8) and (9) in terms of their free and forced response (more precisely, their zero-input and zero-state response). We are now going to argue that $e_y(t)$ and $e_x(t)$ are dominated by their forced response, and that these responses are not affected by setting $w(t) = 1$ for all time.

Inspection of Eq. (9) shows that the forced response of $e_y(t)$ does not depend on the sign of $w(t)$. The same is true for $e_x(t)$, because $e_x(t)$ is the output of a linear time-invariant system which is driven by $e_y(t)$. Only the free responses of these error signals depend on the sign of $w(t)$. The contribution of the free response to the overall solution, however, is relatively small. This follows from the observation that the free response of $e_y(t)$ and $e_x(t)$ consists of brief transients; a new transient is induced each time $w(t)$ changes sign. Since the average time between sign changes of $w(t)$ is long compared to the decay time of the transients, the forced response dominates the overall solution. The corresponding argument for $e_z(t)$ is more difficult. However, our numerical experiments will clearly show that the constraint $w(t) = 1$ leads to an error model which is consistent with the exact error equations.

With $w(t) = 1$, the forced solution to (7) is given by

$$\begin{aligned} e_x(s) &= H_3(s)e_y(s), \\ e_y(s) &= H_{11}(s)P(s) + H_{12}(s)N(s), \\ e_z(s) &= H_{21}(s)P(s) + H_{22}(s)N(s), \end{aligned} \tag{10}$$

where $\mathbf{e}(s)$, $P(s)$, and $N(s)$ denote the Laplace transforms of $\mathbf{e}(t)$, $p(t)$, and $n(t)$ respectively. The transfer functions $H_{ij}(s)$, for $i, j = 1, 2$, correspond

to linear time-invariant systems and are given by

$$H_{11}(s) = \frac{(\bar{z}-r)(s+b)+\sigma_x\sigma_y}{s^2+(b+1)s+b+\sigma_x^2},$$

$$H_{12}(s) = \frac{s+b}{s^2+(b+1)s+b+\sigma_x^2},$$

$$H_{21}(s) = \frac{\sigma_x(\bar{z}-r)-\sigma_y(s+1)}{s^2+(b+1)s+b+\sigma_x^2},$$

$$H_{22}(s) = \frac{\sigma_x}{s^2+(b+1)s+b+\sigma_x^2}.$$

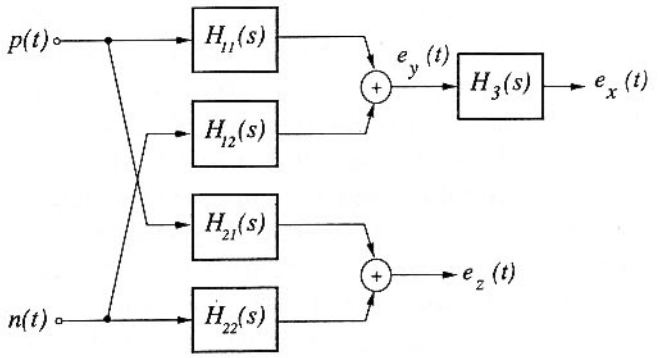

Fig. 8. Equivalent linear time-invariant model of the Lorenz error dynamics.

Equation (10) represents an equivalent linear time-invariant error model which is driven by the perturbation $p(t)$ and white noise $n(t)$. A block diagram representation of (10) is shown in Fig. 8. This system clearly shows that $e_y(t)$ and $e_x(t)$ can be viewed as consisting of the sum of a noise component due to lowpass filtering $n(t)$ and a component due to lowpass filtering the perturbation $p(t)$.

For signal masking and recovery, we are mainly interested in the properties of $H_{11}(s)$ and $H_{12}(s)$. In Figs. 9(a) and 9(b), we show pole-zero plots for

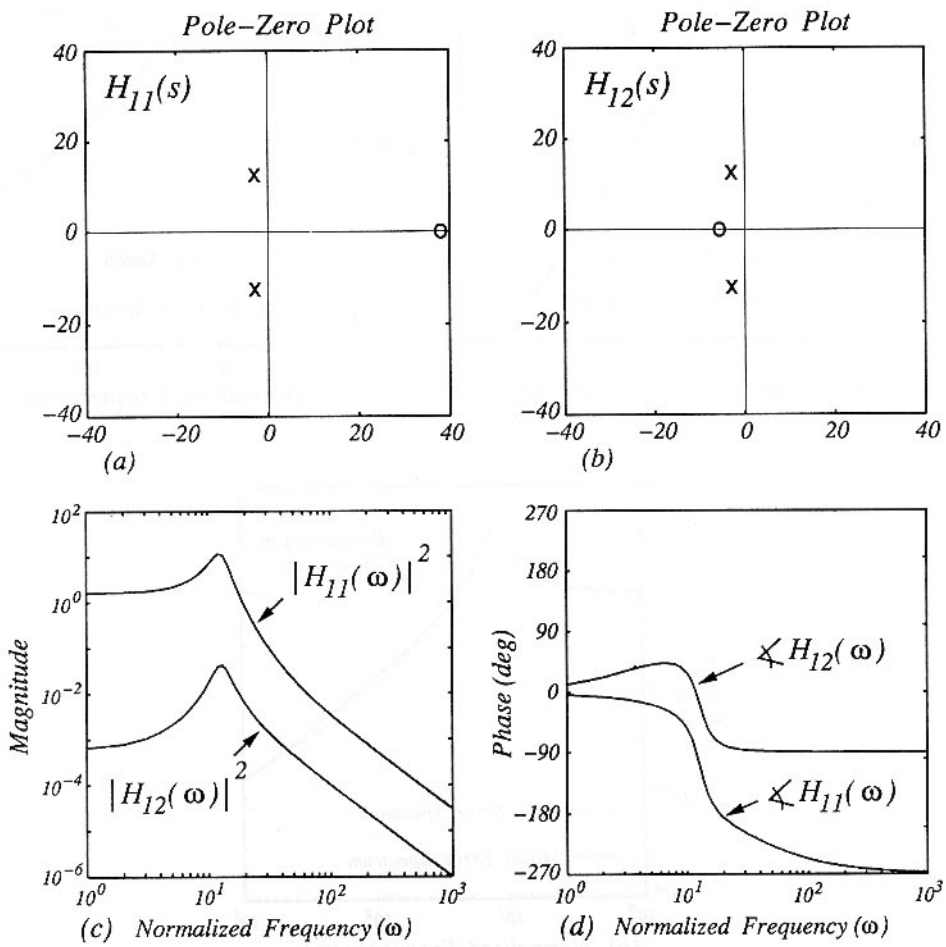

Fig. 9. (a) Pole-zero plot for $H_{11}(s)$. (b) Pole-zero plot for $H_{12}(s)$. (c) Magnitude response of $H_{11}(s)$ and $H_{12}(s)$. (d) Phase response of $H_{11}(s)$ and $H_{12}(s)$.

$H_{11}(s)$ and $H_{12}(s)$ respectively. These transfer functions represent second-order lowpass filters having a cutoff frequency ω approximately equal to 13. The magnitude and phase response of these filters is shown in Figs. 9(c) and 9(d) respectively. Note that $H_{11}(s)$ amplifies signal components within its passband $0 < \omega < 13$, whereas $H_{12}(s)$ attenuates signal components in this frequency range. For messages which are bandlimited to this frequency range, such as the speech sample illustrated in Fig. 3, the error signals $e_y(t)$ and $e_x(t)$ will resemble a slightly amplified and noise-corrupted version of the message. Furthermore, these error signals will be nearly coherent with the message because both $H_{11}(s)$ and $H_3(s)$ exhibit a small group delay in this frequency range.

5. Error Model Performance

In this section, we compare the performance predicted by the error model in Fig. 8 with experimental results. In Sec. 5.1 we consider the case of a perturbation $p(t)$ which is white noise. In Sec. 5.2 we consider $p(t)$ as a speech signal.

5.1. *Additive white noise*

In Fig. 2 we showed the power spectrum of each of the error components as compared with the spectrum of the perturbation and noted that most of the error power is contained in the low frequencies. The error model as depicted in Fig. 8 clearly indicates that each of the error components is the output of a lowpass filter. In Fig. 10 we reproduce

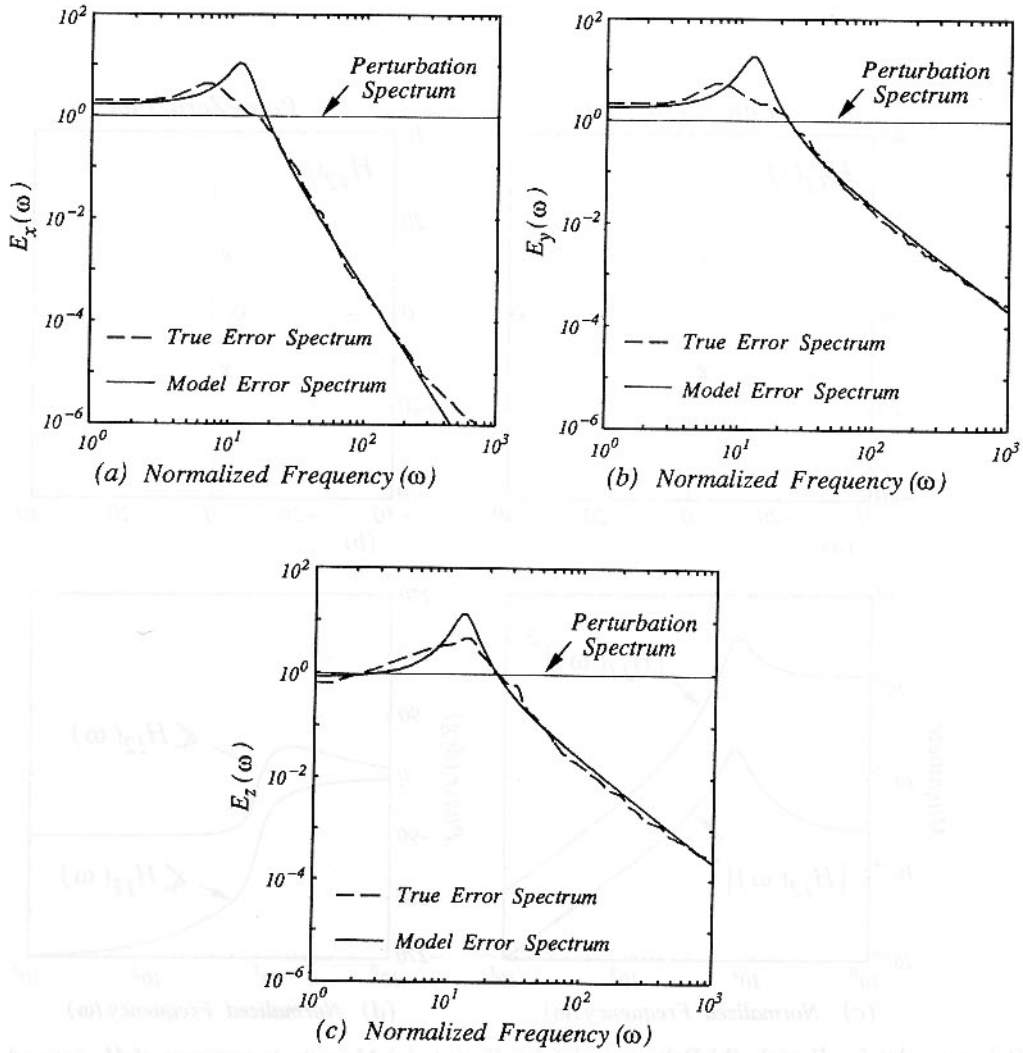

Fig. 10. True and estimated power spectra of the error signals: (a) $E_x(\omega)$. (b) $E_y(\omega)$. (c) $E_z(\omega)$.

Fig. 2 and include the power spectrum of the error components as predicted by the model of Fig. 8. As we see, there is excellent agreement between the true results and the results predicted by the model.

5.2. *Additive speech waveform*

In Fig. 11 we show a block diagram representation of the message recovery process. The recovered message $\hat{p}(t)$ consists of two components, one corresponding directly to the message $p(t)$ and the other corresponding to the error signal $e_x(t)$. We know from the experimental results in Sec. 3 that $\hat{p}(t)$ represents a faithful recovery of $p(t)$. Clearly, if $e_x(t)$ is small relative to $p(t)$, then $\hat{p}(t) \approx p(t)$. However, the assumption that $e_x(t)$ is small is not correct because the low frequency components in $p(t)$ will produce a significant synchronization error. Instead, the explanation is that $e_x(t)$ is not small but is coherent with $p(t)$. This is plausible from Fig. 11 which indicates that $e_x(t)$ consists of the sum of a noise component due to $n(t)$ and a component due to $p(t)$. Because $p(t)$ is relatively low frequency, it can pass through $H_{11}(s)$ and $H_3(s)$ with little phase shift whereas the noise component will be significantly attenuated. Therefore, $e_x(t)$ will resemble a scaled version of $p(t)$ at low frequencies and be noise-like at higher frequencies. This analysis is verified below by numerical experiment.

In Fig. 12(a) we show a comparison of the true and estimated power spectrum of $e_x(t)$. These spectra are consistent and resemble the message spectrum in the frequency range $0 < \omega < 3$. In

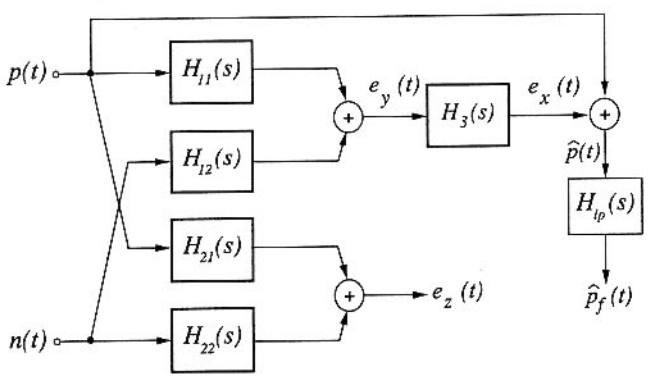

Fig. 11. Dynamical system representation of the message recovery process.

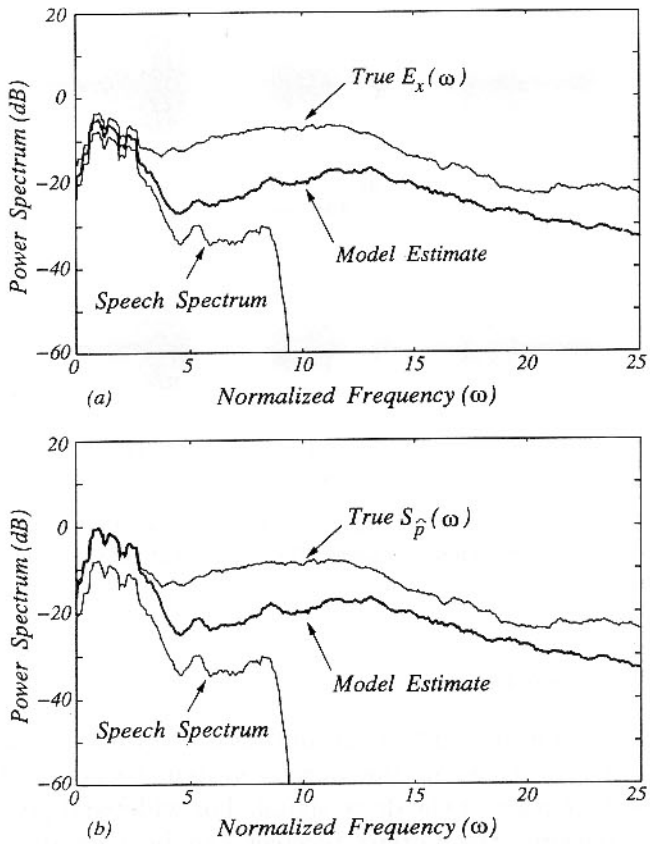

Fig. 12. (a) Power spectrum of $p(t)$ and the true and estimated power spectrum of $e_x(t)$. (b) Power spectrum of $p(t)$ and the true and estimated power spectrum of $\hat{p}(t)$.

Fig. 12(b) we show a comparison of the true and estimated power spectrum of $\hat{p}(t)$. These spectra are also consistent and closely resemble the message spectrum in the frequency range $0 < \omega < 3$. Although the synchronization error $e_x(t)$ is larger than the message $p(t)$, the recovered message $\hat{p}(t)$ resembles a scaled version of $p(t)$ because the message and error are nearly coherent at these frequencies.

To improve the message-to-error ratio of $\hat{p}(t)$, an additional lowpass filter with a transfer function given by

$$H_{\rm lp}(\omega) = \begin{cases} \dfrac{1}{2} & 0 \le \omega \le 3 \text{ rad}, \\ 0 & \omega > 3 \text{ rad}, \end{cases}$$

can be used to process $\hat{p}(t)$. Applying this filter to both the true and estimated $\hat{p}(t)$, we obtain the recovered speech waveforms shown in Fig. 13(a) and Fig. 13(b) respectively. The model estimate is in excellent agreement with the true result.

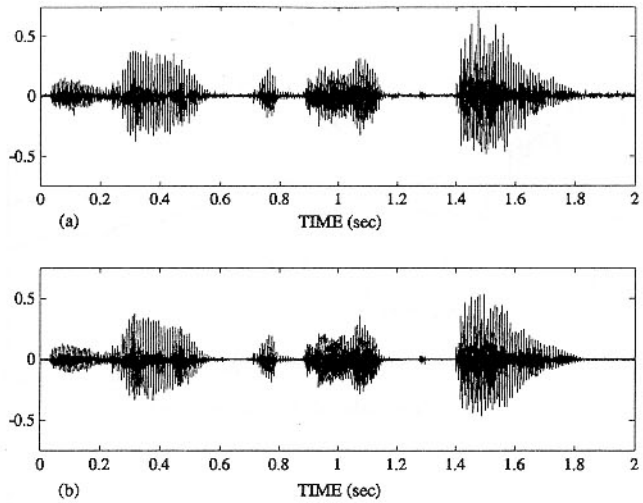

Fig. 13. Speech waveforms: (a) True recovered message. (b) Recovered message using the equivalent linear time-invariant model.

6. Conclusions

This paper examined the question of synchronization robustness in the Lorenz system to additive perturbation of the drive signal. For wideband perturbations, the Lorenz receiver can be viewed as a type of lowpass filter. For perturbations having a lowpass characteristic, such as speech signals, the receiver's synchronization error is coherent with the message at low frequencies. Thus, the receiver's own synchronization error reinforces the original message to allow an accurate recovery of the original message. Experimental evidence for this effect was presented, along with an explanation in terms of an approximate analytical model. These results provide a better understanding of our chaotic signal masking and recovery system.

Acknowledgments

The authors thank Prof. A. S. Willsky for many helpful discussions during various stages of this work. This work was sponsored in part by the Air Force Office of Scientific Research under Grant Number AFOSR-91-0034-A, in part by the National Science Foundation under Grant DMS-9057433, in part by a subcontract from Lockheed Sanders, Inc., under ONR Contract Number N00014-91-C-0125, and in part by the Office of Naval Research under Grant N00014-93-1-0686. K. M. C. gratefully acknowledges support from the M. I. T. Lincoln Laboratory Staff Associate Program.

References

Carroll, T. L. & Pecora, L. M. [1991] "Synchronizing chaotic circuits," *IEEE Trans. Circuits Systems* **38**, 453–456.

Cuomo, K. M. & Oppenheim, A. V. [1993] "Chaotic signals and systems for communications," in *Proc. 1993 IEEE ICASSP* **III**.

Cuomo, K. M. & Oppenheim, A. V. [1993] "Circuit implementation of synchronized chaos with applications to communications," *Phys. Rev. Lett.* **71**, 65–68.

Cuomo, K. M., Oppenheim, A. V. & Strogatz, S. H. [1993] "Synchronization of Lorenz-based chaotic circuits with applications to communications," To appear in *IEEE Trans. Circuits Systems.*

Kocarev, Lj., Halle, K. S., Eckert, K. & Chua, L. O. [1992] "Experimental demonstration of secure communications via chaotic synchronization," *Int. J. Bifurcation and Chaos* **2**(3), 709–713.

Oppenheim, A. V., Wornell, G. W., Isabelle, S. H. & Cuomo K. M. [1992] "Signal processing in the context of chaotic signals," in *Proc. 1992 IEEE ICASSP* **IV**, 117–120.

Pecora, L. M. & Carroll, T. L. [1990] "Synchronization in chaotic systems," *Phys. Rev. Lett.* **64**, 821–823.

Pecora, L. M. & Carroll, T. L. [1991] "Driving systems with chaotic signals," *Phys. Rev.* **A44**, 2374–2383.